Classification of Cervical Intraepithelial Neoplasia Based on Combination of GLCM and L*a*b* on Colposcopy Image Using Machine Learning

Zendi Zakaria Raga Permana
School of Electrical Engineering and Informatics
Institut Teknologi Bandung
Bandung, Indonesia
23222319@std.stei.itb.ac.id

Agung Wahyu Setiawan
School of Electrical Engineering and Informatics
Institut Teknologi Bandung
Bandung, Indonesia
awsetiawan@itb.ac.id

Abstract—Colposcopy can potentially improve diagnostic capabilities to guide cervical biopsies, contributing to improved cervical cancer screening. The previous study compared diagnostic accuracy in histologic CIN between senior and junior colposcopists, the senior colposcopists showing higher sensitivity but lower specificity than the junior. This research has significantly contributed to categorizing CIN1, CIN2, and CIN3 by utilizing features extracted from GLCM and L*a*b* color spaces, using machine learning techniques to aid cervical pre-cancer diagnosis. Three machine learning tools were random forest, decision tree, and extra trees. The results of this study have shown that the extra tress classifier has the best performance value by using six GLCM features: contrast, correlation, energy, homogeneity, dissimilarity, asm, and one L*a*b* feature, namely median_l. The performance results have improved to 0.98 accuracy, 0.97 sensitivity, and 0.98 specificity. Processing CIN1 data on GLCM features took an average of 20.70 s and L*a*b* for 21.74 s. The processing of CIN2 data on GLCM features is 27.57 s, and L*a*b* is 27.37 s. The processing of CIN3 data on GLCM is 31.22 s, and L*a*b* is 31.38 s. In aggregate, the lowest average processing time using the GLCM features was 26.20 s. Based on the testing results, this research produces an FNR of 0.015, which indicates that this research in the future, when applied to medical care, has a slight possibility of diagnostic errors. Abnormal vascular features such as punctation and mosaic are the only significant if visible in limited acetowhite areas, making it challenging for researchers to select more appropriate features.

Index Terms—colposcopy images, classification, cervical cancer, GLCM, L*a*b*, machine learning

I. INTRODUCTION

Cervical cancer constitutes a significant international public health issue, holding the position as the fourth most prevalent malignancy among females worldwide. Approximately 527,624 women are diagnosed with cervical cancer each year, resulting in 265,672 fatalities attributed to this disease. Moreover, cervical cancer contributes to 4% of global cancer diagnoses [1]. The predominant etiological factor responsible for almost all instances of cervical cancer is Human Papillomavirus (HPV) infection. HPV is unequivocally linked to nearly every case of cervical cancer. While HPV tests demonstrated superior sensitivity when compared to cytology

(96.1% vs. 53.0%) and specificity (90.7% vs. 96.3%) [2]. Consequently, the cytology component contributed to merely five cases per million women per year [3]. The screening protocol for cervical cancer adheres to a standardized workflow encompassing HPV testing, cytology (commonly referred to as PAP smear testing), colposcopy, testing, and biopsy [4].

Colposcopy is a widely adopted surgical intervention aimed at preventing cervical cancer. The prompt detection and accurate classification of this form of cancer can substantially enhance the overall clinical management of patients [5]. Numerous research endeavors have explored diverse methodologies for extracting colposcopy images [6]–[8]. The presence of pathological regions can serve as potential indicators of neoplastic conditions. These anomalous areas include acetowhite changes, irregular vascular patterns, mosaic patterns, and punctate lesions [9], [10]. Several studies have explored Cervical Intraepithelial Neoplasia (CIN) and its classifications [11]–[13].

Previous studies have applied essential features to the classification process, including the Gray Level Co-occurrence Matrix (GLCM) and L*a*b*. Utilizing GLCM proves to be a potent method for scrutinizing texture characteristics, enabling the extraction of various texture features, such as contrast, correlation, entropy, uniformity, energy, and more, from the source image of cervical cancer [14]. Previous research extracted 13 Haralick features for each GLCM [15]. Sukumar et al. have performed feature extraction for pap smear images in classifying normal and abnormal cervical cancer detection. Some features include GLCM, law's texture feature, wavelet, and Local Binary Pattern (LBP) [16].

Cervigram images have been extracted with L*a*b* color space features, Histogram of Oriented Gradients (HOG), and LBP. Furthermore, classification is performed using a Convolutional Neural Network (CNN), and the results are accuracy: 78.41%, sensitivity: 80.87%, and specificity: 75.94% [17]. Other studies have also applied CNN, Support Vector Machine (SVM), Random Forest (RF), Adaboost, Gradient Boosting (GB), Decision Tree (DT), and k-Nearest Neighbor (k-NN) for cervical cancer classification [18], [19]. Based on the im-
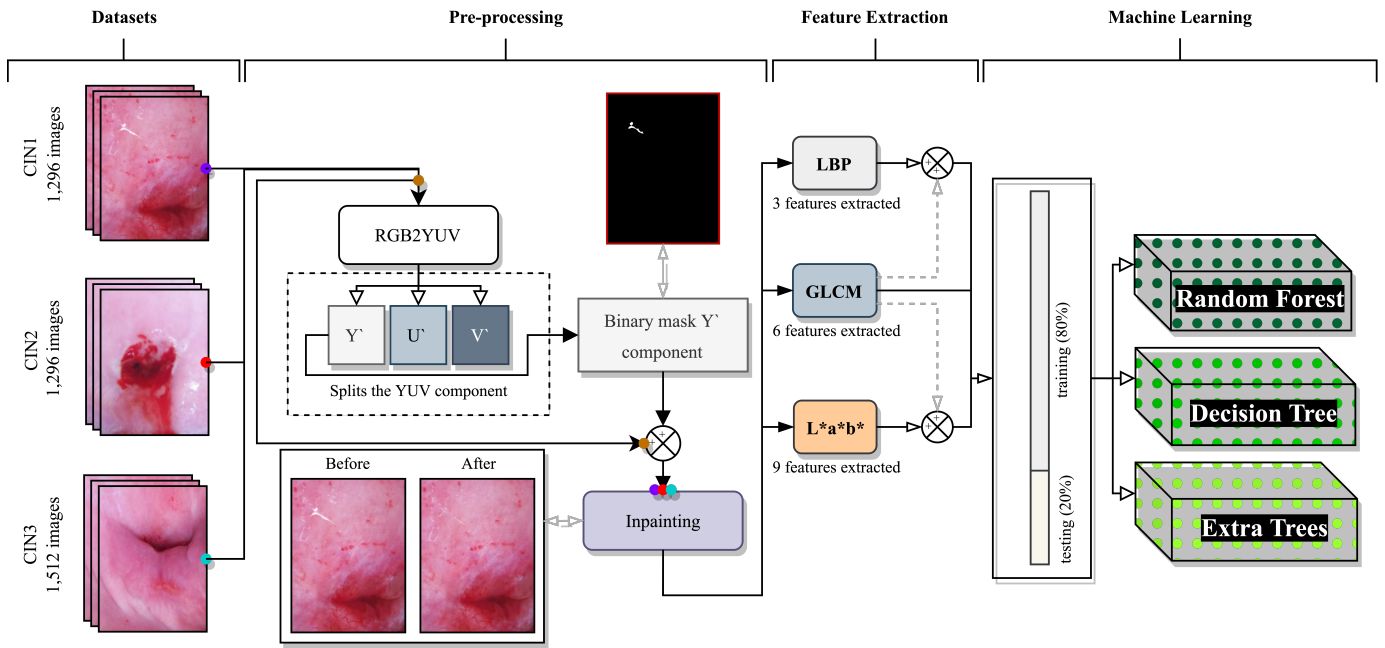
Fig. 1. The proposed method including preprocessing (binary masking and inpainting), feature extraction process (GLCM, LBP, and L*a*b*), and classsification process (RF, DT, and ET).

portance of early detection and preventive measures to prevent cervical cancer, this study has contributed to classifying the CIN category based on the feature results from GLCM and L*a*b* by applying machine learning to determine the CIN category to help diagnose cervical pre-cancer.

II. RELATED WORK

An automated machine vision system for the histological grading of CIN was introduced [20]. Previous investigations focused on localized and automated analysis of histological images of the cervix to identify the degree of CIN. Notable improvements include GLCM features such as contrast, correlation, dissimilarity, entropy, homogeneity, and angular second moment (ASM), in addition to area-based features. However, it is essential to note that the limited sample size precludes deriving conclusive findings regarding the efficacy of the proposed methodology [14]. Color assumes a pivotal role in the classification of cervical lesions, given that one of the foremost visual attributes of the cervix with significant diagnostic relevance is the presence of acetowhitening regions. In conjunction with color and gradient attributes, a novel addition to the feature set incorporates a LBP feature, which adeptly captures localized textural characteristics to aid cervical lesion classification. Notably, Ojala et al. initially demonstrated the efficacy of LBP in texture classification [21].

Anwer et al. introduced a method to predict and identify specular highlights within digital images, accurately delineating the regions affected by highlighting and assigning appropriate labels. Remarkably, the training duration for this model was notably reduced to just 40 minutes compared to the pre-existing methods [22]. Another study introduced an innovative fuzzy reasoning model that leveraged temporal grayscale and texture attributes within the acetowhite region during an acetic acid test to classify CIN. The result of this study was a sensitivity of 85.9% and specificity of 86.6% [12]. Numerous approaches have been explored for the analysis of cervical images. Multi-parameter magnetic resonance imaging, in conjunction with machine learning, has been employed to automate the interpretation of colposcopic images [23]. A method used CNN with extreme learning machines to classify cervical cancer [9]. A comprehensive review of image analysis techniques and a machine learning-based framework for automated cervical cancer screening using cervical smear images was introduced [24]. However, the methodology outlined above relies primarily on cervical images. While cervical images play a significant role in treating cervical cancer, it is crucial to recognize that certain modifiable factors associated with this condition can be predicted during the initial screening stage at a relatively low cost.

III. PROPOSED METHOD

This study uses a Kaggle dataset with dimensions of 277×369 px and a resolution of 100×100 dpi. This dataset contained 4,104 images divided into 1,296 CIN1, 1,296 CIN2, and 1,512 CIN3 categories [25]. The initial challenge when using this dataset are that each illustration has specular reflections around the cervical area, and the different locations of reflection. Therefore, this study pre-processed the specular reflection detection using binary masking by utilizing RGB to YUV image color space conversion and separated the YUV components into Y', U', and V'. The Y' component alone does not have specular reflection information, which makes

Scheme	Feature Extractions	Feature Selections	Model	Accuracy	Sensitivity	Specificity
#1	GLCM	contrast, correlation, energy, homogeneity, dissimilarity, asm [6 features]	DT	0.89	0.85	0.93
#2	GLCM	contrast, correlation, energy, homogeneity, dissimilarity, asm [6 features]	RF	0.93	0.90	0.95
#3	GLCM	contrast, correlation, energy, homogeneity, dissimilarity, asm [6 features]	ET	0.96	0.95	0.97
#4	GLCM-LBP	contrast, correlation, energy, homogeneity, dissimilarity, asm, median_lbp, ptp_lbp, std_lbp [9 features]	DT	0.68	0.72	0.80
#5	GLCM-LBP	contrast, correlation, energy, homogeneity, dissimilarity, asm, median_lbp, ptp_lbp, std_lbp [9 features]	RF	0.75	0.80	0.65
#6	GLCM-LBP	contrast, correlation, energy, homogeneity, dissimilarity, asm, median_lbp, ptp_lbp, std_lbp [9 features]	ET	0.81	0.84	0.75
#7	GLCM-L*a*b*	contrast, correlation, energy, homogeneity, dissimilarity, asm, median_l, median_a, median_b, ptp_l, ptp_a, ptp_b, std_l, std_a, std_b [15 features]	DT	0.82	0.85	0.75
#8	GLCM-L*a*b*	contrast, correlation, energy, homogeneity, dissimilarity, asm, median_l, median_a, median_b, ptp_l, ptp_a, ptp_b, std_l, std_a, std_b [15 features]	RF	0.93	0.96	0.87
#9	GLCM-L*a*b*	contrast, correlation, energy, homogeneity, dissimilarity, asm, median_l, median_a, median_b, ptp_l, ptp_a, ptp_b, std_l, std_a, std_b [15 features]	ET	0.95	0.96	0.93
#10	GLCM-LBP	contrast, correlation, energy, homogeneity, dissimilarity, asm, ptp_lbp, std_lbp [8 features]	ET	0.83	0.89	0.73
#11	GLCM-L*a*b*	contrast, correlation, energy, homogeneity, dissimilarity, asm, median_l [7 features]	ET	**0.98**	**0.97**	**0.98**

it easier to perform binary masking of specular reflection [26]. Following the specular reflection detection stage, binary masking coordinates are used for image enhancement using the inpainting method. After the pre-processing stage, in performing CIN classification, it is necessary to select feature extraction to obtain image information on texture, color, and cervical lesions.

Referring to the colposcopic examination procedure to determine whether the cervix is in the CIN1, CIN2, or CIN3 category by swede score assessment, five parameters of cervical features are needed, namely aceto uptake, margins, vessels, lesions, and iodine uptake [27]. Therefore, this study proposes using a combination of features from GLCM, LBP, and L*a*b* and determines the most appropriate and best features to improve the performance of the classification model. In this study, the GLCM parameters are dissimilarity, correlation, homogeneity, contrast, ASM, and energy. Determination of texture in LBP is done by determining parameters by calculating the median value, standard deviation (std), and peak-to-peak (ptp). Then, L*a*b* is separated into L*', a*', and b*' components [28]. Each component is calculated based on the median, std, and ptp values.

Following all the feature extraction processes, it is necessary to separate the training and test data, so in this study, 80% of the training data and 20% of the test data are performed. The training data will be trained with the specified model including RF, DT, and ET. The training in this study performs a combination of schemes to see the performance of each model. Then, 20% of the test data is tested by evaluating the metrics on the three models. The block diagram of the proposed method can be seen in Fig. 1.

IV. RESULT AND DISCUSSION

This chapter describes the results of feature testing, feature selection, and classification. The 18 features have been extracted, including GLCM (contrast, correlation, energy, homogeneity, dissimilarity, and ASM), LBP (median_lbp, ptp_lbp, and std_lbp), and L*a*b* (median_l, median_a, median_b, ptp_l, ptp_a, ptp_b, and std_l, std_a, and std_b). The selection of these features refer to several previous studies [14], [16], [18]. The GLCM features, including contrast, have an average value of 288.49±167.50, correlation value of 0.96±0.02, energy value of 0.13±0.06, homogeneity value of 0.29±0.07, dissimilarity value of 7.89±2.48, ASM value of 0.02±0.01. The average value of LBP features includes median_lbp of 205.78±22.35, ptp_lbp of 255±0, and std_lbp of 86.48±3.17. The mean values of L*a*b* features include median_l of 241.73±101.24, median_a of 0, median_b of 0.008±0.22, ptp_l of 15317.33±6569.71, ptp_a of 17543.84±6499.01, ptp_b of 18570.42±5530.67, and std_l of 1033.45±336.36, std_a of 1420.37±290.07, std_b of 1659.09±319.740. Fig. 2. shows the distribution results of all extracted features on CIN1, CIN2, and CIN3.

This study also discusses the processing time required to process features from each method on each dataset. Fig. 3 shows the time performance data of GLCM, L*a*b*, and LBP at 20 iterations. The processing of CIN1 data on GLCM features takes an average time of 20.70 s, L*a*b* for 21.74 s, and LBP for 2,012.81 s. The processing of CIN2 data on GLCM features takes an average time of 27.57 s, L*a*b* for 27.37 s, and LBP for 2,561. 63 s. The processing of CIN3 data on GLCM features takes an average time of 31.22 s, L*a*b* for 31.38 s, and LBP for 2,645.69 s. Overall, the
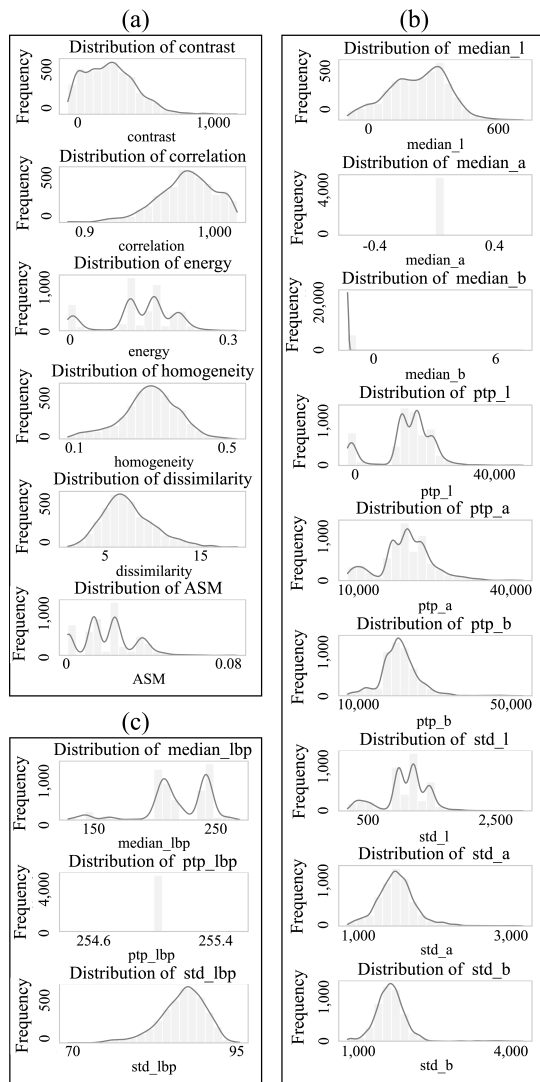
Fig. 2. The distribution of feature extraction in this study, including (a) GLCM is divided into contrast, correlation, energy, homogeneity, dissimilarity, and ASM. (b) L*a*b* is divided into median_l, median_a, median_b, ptp_l, ptp_a, ptp_b, and std_l, std_a, std_b. (c) LBP is divided into median_lbp, ptp_lbp, and std_lbp.

Fig. 3. The graph of feature extraction performance of CIN1, CIN2, and CIN3.

lowest average processing time using GLCM features is 26.20 s. There are 11 scheme models of this research shown in Table I.

The highest performance value resulted using scheme #11, which combines GLCM and L*a*b* features with a total of seven features using the Extra Trees classifier, resulting in an accuracy value of 0.98, sensitivity of 0.97, and specificity of 0.98. Fig. 4 shows the comparison metric on CIN1, CIN2, and CIN3 in scheme #11. Fig. 5 shows the results of training and testing on scheme #11. Based on the testing results, this research produces a False Negative Rate (FNR) of 0.015, which indicates that this research in the future, when applied to medical care, has a slight possibility of diagnostic errors. Following research on biomedical diagnostics, a small FNR value is significant [29]. Fig.6 shows the Receiver Operating
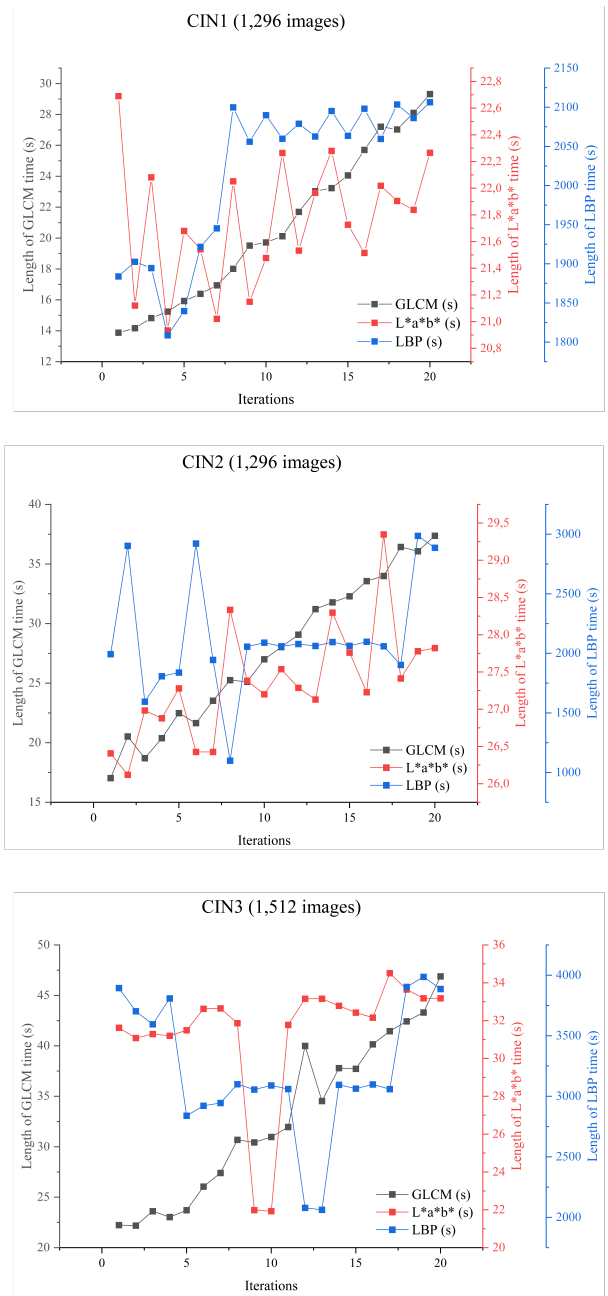
Characteristic (ROC) curve resulting from scheme #11 by comparing three classifiers, namely Random Forest, Decision Tree, and Extra Trees. Based on the graph, the highest actual positive rate is generated by Extra Trees, showing a small false positive rate. Several previous studies have applied ROC graphs to evaluate the research results on colposcopy images [30]. Previous research has used the Inception-ResNet-V2 method, which resulted in an accuracy of 0.69, sensitivity of 0.66, and specificity of 0.70 [13].

Previous research using the ColpoNet method yielded an accuracy of 0.81 [6]. Dash et al. introduced a multiple-scale
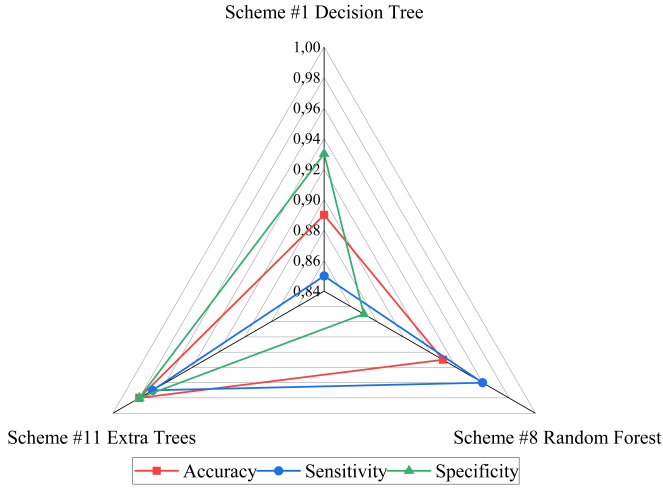
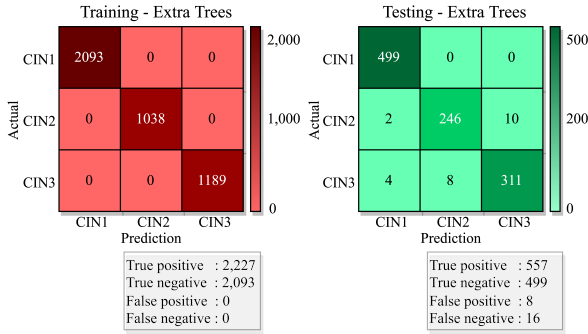Fig. 4. Radar visualization of the classification results.

Fig. 5. The confusion matrix in CIN1, CIN2, and CIN3 using the ET classifier based on Scheme#11.

TABLE II
COMPARISON OF THE METHODS IN THIS STUDY WITH SOME PREVIOUS
STUDIES.

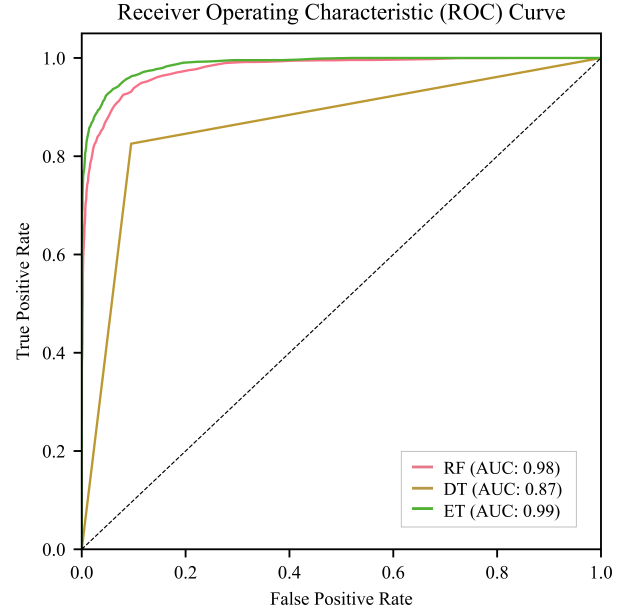| Ref	Method	Datasets	Metrics
[13]	Inception-ResNet-V2	43 cancer images, 311 CIN3 images, 211 CIN2 images, 100 CIN1 images, and 126 normal images.	Accuracy: 0.69 Sensitivity: 0.66 Specificity: 0.70
[6]	ColpoNet	280 images of CIN1/Normal, 280 images of CIN2/CIN3/CIN4.	Accuracy: 0.81
[31]	Inception-Resnet-V2	CIN1: 169, CIN2: 43, and CIN3: 80.	Accuracy: 0.81 Sensitivity: 0.81 Specificity: 0.90
[32]	DenseNet-121	4,870 images (include CIN1, CIN2, and CIN3).	Accuracy: 0.97 Sensitivity: 0.92 Specificity: 0.94
[25]	DenseNet-161 and ResNet-152	Intel & MobileODT Cervical Cancer Screening (Kaggle Competition)	Log loss: 0.76
Proposed method	GLCM-L*a*b*-ET	1,296 images of CIN1, 1,296 images of CIN2, and 1,512 images of CIN3.	Accuracy: 0.98 Sensitivity: 0.97 Specificity: 0.98 Log loss: 0.20

Fig. 6. The ROC curve generated using the scheme#11.

feature fusion method using Inception-Resnet-V2, resulting in an accuracy of 0.81, sensitivity of 0.81, and specificity of 0.90. This cervical cancer screening approach circumvents the need for a biopsy, in which a tissue sample is necessary for analysis 31. Another study using the same dataset as this study resulted in an accuracy value of 0.97, sensitivity of 0.92, and specificity of 0.94. This previous approach uses binary masking to detect the glare region, and a finely adjusted U-Net model is applied for segmentation [32]. Furthermore, compared to the results of the Kaggle competition winner getting an evaluation using a log loss of 0.76963 [25], this study obtained a log loss value of 0.20981. This research produces higher performance values than some previous studies shown in Table II.

V. CONCLUSION

The classification performance results of CIN1, CIN2, and CIN3 strongly depend on the features used. This research has pre-processed specular reflection detection using binary masking by utilizing RGB to YUV image color space conversion and separating YUV components into Y', U', and V'. The next step is to have extracted features using LBP, GLCM, and L*a*b*. The combination of features to produce the highest performance value resulted from GLCM and L*a*b*. Evaluation of the performance of the three classifiers of this study using the ROC graph. The AUC (Area Under the Curve) indicates the classifier's discriminative capability in classification tasks. The AUC value on the RF is 0.98, the DT is 0.87, and the ET is 0.99. Our future research will develop a real-time system for diagnosing cervical cancer on colposcopy images.

REFERENCES

[1] T. A. Kessler, "Cervical cancer: prevention and early detection," in *Seminars in oncology nursing*, vol. 33, no. 2. Elsevier, 2017, pp. 172–183.

[2] J. Cuzick, C. Clavel, K.-U. Petry, C. J. Meijer, H. Hoyer, S. Ratnam, A. Szarewski, P. Birembaut, S. Kulasingam, P. Sasieni *et al.*, "Overview of the european and north american studies on hpv testing in primary cervical cancer screening," *International journal of cancer*, vol. 119, no. 5, pp. 1095–1101, 2006.

[3] N. Bhatla and S. Singhal, "Primary hpv screening for cervical cancer," *Best Practice & Research Clinical Obstetrics & Gynaecology*, vol. 65, pp. 98–108, 2020.

[4] D. M. Eddy, "Screening for cervical cancer," *Annals of internal medicine*, vol. 113, no. 3, pp. 214–226, 1990.

[5] V. Chandran, M. Sumithra, A. Karthick, T. George, M. Deivakani, B. Elakkiya, U. Subramaniam, S. Manoharan *et al.*, "Diagnosis of cervical cancer based on ensemble deep learning network using colposcopy images," *BioMed Research International*, vol. 2021, 2021.

[6] S. K. Saini, V. Bansal, R. Kaur, and M. Juneja, "Colponet for automated cervical cancer screening using colposcopy images," *Machine Vision and Applications*, vol. 31, pp. 1–15, 2020.

[7] Y. Li, J. Chen, P. Xue, C. Tang, J. Chang, C. Chu, K. Ma, Q. Li, Y. Zheng, and Y. Qiao, "Computer-aided cervical cancer diagnosis using time-lapsed colposcopic images," *IEEE transactions on medical imaging*, vol. 39, no. 11, pp. 3403–3415, 2020.

[8] M. Sato, K. Horie, A. Hara, Y. Miyamoto, K. Kurihara, K. Tomio, and H. Yokota, "Application of deep learning to the classification of images from colposcopy," *Oncology letters*, vol. 15, no. 3, pp. 3518–3523, 2018.

[9] A. Ghoneim, G. Muhammad, and M. S. Hossain, "Cervical cancer classification using convolutional neural networks and extreme learning machines," *Future Generation Computer Systems*, vol. 102, pp. 643–649, 2020.

[10] J. Lu, E. Song, A. Ghoneim, and M. Alrashoud, "Machine learning for assisting cervical cancer diagnosis: An ensemble approach," *Future Generation Computer Systems*, vol. 106, pp. 199–205, 2020.

[11] O. E. Aina, S. A. Adeshina, A. P. Adedigba, and A. M. Aibinu, "Classification of cervical intraepithelial neoplasia (cin) using fine-tuned convolutional neural networks," *Intelligence-Based Medicine*, vol. 5, p. 100031, 2021.

[12] J. Liu, Y. Peng, and Y. Zhang, "A fuzzy reasoning model for cervical intraepithelial neoplasia classification using temporal grayscale change and textures of cervical images during acetic acid tests," *Ieee Access*, vol. 7, pp. 13 536–13 545, 2019.

[13] B.-J. Cho, Y. J. Choi, M.-J. Lee, J. H. Kim, G.-H. Son, S.-H. Park, H.-B. Kim, Y.-J. Joo, H.-Y. Cho, M. S. Kyung *et al.*, "Classification of cervical neoplasms on colposcopic photography using deep learning," *Scientific reports*, vol. 10, no. 1, p. 13652, 2020.

[14] L. Wei, Q. Gan, and T. Ji, "Cervical cancer histology image identification method based on texture and lesion area features," *Computer Assisted Surgery*, vol. 22, no. sup1, pp. 186–199, 2017.

[15] S. Nehra, J. L. Raheja, K. Butte, and A. Zope, "Detection of cervical cancer using glcm and support vector machines," in *2018 6th Edition of International Conference on Wireless Networks & Embedded Systems (WECON)*. IEEE, 2018, pp. 49–53.

[16] P. Sukumar and R. Gnanamurthy, "Computer aided detection of cervical cancer using pap smear images based on adaptive neuro fuzzy inference system classifier," *Journal of Medical Imaging and Health Informatics*, vol. 6, no. 2, pp. 312–319, 2016.

[17] T. Xu, H. Zhang, C. Xin, E. Kim, L. R. Long, Z. Xue, S. Antani, and X. Huang, "Multi-feature based benchmark for cervical dysplasia classification evaluation," *Pattern recognition*, vol. 63, pp. 468–475, 2017.

[18] Y. Yu, J. Ma, W. Zhao, Z. Li, and S. Ding, "Msci: A multistate dataset for colposcopy image classification of cervical cancer screening," *International journal of medical informatics*, vol. 146, p. 104352, 2021.

[19] Z. Z. R. Permana and A. W. Setiawan, "Research challenges in cervical cancer segmentation and classification using colposcopy images," in *2023 10th International Conference on Information Technology, Computer, and Electrical Engineering (ICITACEE)*, 2023, pp. 371–376.

[20] S. J. Keenan, J. Diamond, W. Glenn McCluggage, H. Bharucha, D. Thompson, P. H. Bartels, and P. W. Hamilton, "An automated machine vision system for the histological grading of cervical intraepithelial neoplasia (cin)," *The Journal of pathology*, vol. 192, no. 3, pp. 351–362, 2000.

[21] T. Ojala, M. Pietikäinen, and D. Harwood, "A comparative study of texture measures with classification based on featured distributions," *Pattern recognition*, vol. 29, no. 1, pp. 51–59, 1996.

[22] A. Anwer, S. Ainouz, M. N. M. Saad, S. S. A. Ali, and F. Meriaudeau, "Specseg network for specular highlight detection and segmentation in real-world images," *Sensors*, vol. 22, no. 17, p. 6552, 2022.

[23] T. Torheim, E. Malinen, K. H. Hole, K. V. Lund, U. G. Indahl, H. Lyng, K. Kvaal, and C. M. Futsaether, "Autodelineation of cervical cancers using multiparametric magnetic resonance imaging and machine learning," *Acta oncologica*, vol. 56, no. 6, pp. 806–812, 2017.

[24] W. William, A. Ware, A. H. Basaza-Ejiri, and J. Obungoloch, "A review of image analysis and machine learning techniques for automated cervical cancer screening from pap-smear images," *Computer methods and programs in biomedicine*, vol. 164, pp. 15–22, 2018.

[25] I. MobileODT, "Intel & mobileodt cervical cancer screening," 2017.

[26] B. Bai, P.-Z. Liu, Y.-Z. Du, and Y.-M. Luo, "Automatic segmentation of cervical region in colposcopic images using k-means," *Australasian physical & engineering sciences in medicine*, vol. 41, pp. 1077–1085, 2018.

[27] M. J. Khan, C. L. Werner, T. M. Darragh, R. S. Guido, C. Mathews, A.-B. Moscicki, M. M. Mitchell, M. Schiffman, N. Wentzensen, L. S. Massad *et al.*, "Asccp colposcopy standards: role of colposcopy, benefits, potential harms, and terminology for colposcopic practice," *Journal of lower genital tract disease*, vol. 21, no. 4, pp. 223–229, 2017.

[28] A. W. Setiawan, A. Faisal, N. Resfita, and Y. A. Rahman, "Detection of malaria parasites using thresholding in rgb, ycbcr and lab color spaces," in *2021 International Seminar on Application for Technology of Information and Communication (iSemantic)*, 2021, pp. 70–75.

[29] Y. Liu, J. Liao, X. Yi, Z. Pan, J. Pan, C. Sun, H. Zhou, and Y. Meng, "Diagnostic value of colposcopy in patients with cytology-negative and hr-hpv-positive cervical lesions," *Archives of Gynecology and Obstetrics*, vol. 306, no. 4, pp. 1161–1169, 2022.

[30] T. Zhang, Y.-m. Luo, P. Li, P.-z. Liu, Y.-z. Du, P. Sun, B. Dong, and H. Xue, "Cervical precancerous lesions classification using pre-trained densely connected convolutional networks with colposcopy images," *Biomedical signal processing and control*, vol. 55, p. 101566, 2020.

[31] S. Dash, P. K. Sethy, and S. K. Behera, "Cervical transformation zone segmentation and classification based on improved inception-resnet-v2 using colposcopy images," *Cancer Informatics*, vol. 22, p. 11769351231161477, 2023.

[32] M. J. Susan and P. Subashini, "Improvising grading of cervical cancer using quality assessment method in smart colposcopy images," *Measurement: Sensors*, p. 100788, 2023.